Bioprinting 14 (2019) e00047

Contents lists available at ScienceDirect

Bioprinting

journal homepage: www.elsevier.com/locate/bprint

Physics of cellular self-assembly– a microscopic model and mathematical framework for faster maturation of bioprinted tissues

Ashkan Shafiee [a,*], Elham Ghadiri [a,b], David Williams [a], Anthony Atala [a]

[a] Wake Forest Institute for Regenerative Medicine, Wake Forest School of Medicine, Winston-Salem, NC, 27101, USA
[b] Department of Chemistry, Wake Forest University, Winston-Salem, NC, 27109, USA

ARTICLE INFO

Keywords:
Bioprinting
Zipper model
Dynamics of cell adhesion molecules
Energy of cellular self-assembly
Tissue maturation

ABSTRACT

Bioprinting of autologous tissues encompasses many different steps, and accelerating the procedure can be critical for patients with an urgent need of organs. The physical aspects of self-assembly and the dynamics of multicellular systems used with printing technologies for tissue fabrication are therefore very important. We have developed a microscopic model based on the dynamics of cell adhesion molecules. Here, the general model is described for different bioink geometries. Furthermore, a mathematical framework is established, based on statistical mechanics, to investigate tissue fusion, which is an essential element of the self-assembly phenomenon during tissue maturation in the post-bioprinting procedure. Using the mathematical framework and microscopic model, the interactions at the cellular level in the maturation of bioprinted tissues have been investigated. The fusion of tissue-like cell aggregates (cellular bioinks) is elaborated with the help of bonds among their adhesion molecules. Statistical mechanics and the zipper model are used to describe the fusion procedure. Consequently, the partition function for the zipper model and the system energy are calculated and compared in order to understand the effect of bioink geometries on the acceleration of the maturation of bioprinted tissues. Based on our microscopic model and mathematical formulation, we introduce some topological criteria for bioinks for faster maturation of bioprinted tissues.

1. Introduction

Advanced printing technologies have been employed extensively in many different fields, ranging from energy harvesting [1–3] and printed electronics [4–7], to biomedical applications [8,9] and biosensing [10–12]. Among other fields, tissue engineering has benefited the most from scalability, precision, and reproducibility of bioprinting; as such, bioprinting has become one of the most effective biofabrication techniques [13–15]. In autologous tissue engineering patients' cells are used to regenerate human tissues or organs that eliminate the chance of organ rejection [16]. Nevertheless, there is a lengthy procedure including biopsy, isolation, and proliferation of the cells, as well as biofabrication, followed by implanting mature/ready tissues. This long procedure can be life-threatening for patients in urgent need of new organs. Therefore, accelerating each step of the lengthy, tedious, and costly tissue printing process would be extremely beneficial for patients with end-stage organ failure.

There are two major approaches in tissue engineering: scaffold-based and scaffold-free [16]. In scaffold-free tissue engineering, cellular materials are used, and the science and principles of self-assembly as well as the dynamics of multicellular systems are employed [17,18]. This method involves high cell density printing without any biomaterial, which makes it favorable for real tissue fabrications. Scaffold-free tissue engineering has benefited from prior investigations in embryonic development focused on the mechanical aspects of multicellular dynamics, which are principles that can be applied to bioprinting [19–21]. In the scaffold-free tissue engineering approach, cells are provided with the environment similar to their natural condition in the body, enabling them to recapitulate their in vivo multicellular behavior and self-assembly. However, there are still indications in the bioprinting procedure to be understood in order to enhance the quality of the bioprinted products associated with the lower costs and shorter times of the procedure. It is worth noting that the difference between 3D bioprinting and 3D printing of ordinary objects is in the post-printing process. In general, a 3D-printed object is usually ready for use immediately. However, a bioprinted structure must be mature prior to implantation. The fourth dimension of bioprinting, "time," lets the bioprinted biological structure reach the mature stage needed for an intermediate bioreactor

* Corresponding author.
E-mail address: ashafiee@wakehealth.edu (A. Shafiee).

https://doi.org/10.1016/j.bprint.2019.e00047
Received 8 February 2019; Received in revised form 7 March 2019; Accepted 8 March 2019

step, or for actual in vivo implantation. The maturation stage may involve self-assembly steps, such as cell sorting, and tissue fusion, that make the biological structure durable enough for transferring to the bioreactor – that provides an appropriate physiological condition for further maturation [22]. The physical principals of self-assembly in multicellular systems have been used to predict the time for this process in bioprinted tissues [23,24].

Tissue fusion is one of the most critical self-assembly phenomena observed in embryonic development. It is the corollary of the differential adhesion hypothesis established by Steinberg in 1963, which stated that different cells show different adhesions to each other as their inherent properties. Fusion of tissue like cell aggregates or bioinks is driven by the apparent tissue surface tension (γ) and is resisted by tissue viscosity (η) [22–24]. Apparent tissue surface tension and tissue viscosity are some of the biomechanical parameters that are employed to investigate tissue behavior based on an analogy between tissues and liquids known as "tissue liquidity" [16,25,26]. Fusion is one of the most important phenomena during tissue maturation and can be investigated quantitatively by the characteristic fusion time, using the equation $\tau = \eta R_0/\gamma$, where τ, γ, η, and R_0 are characteristic fusion time, tissue surface tension, tissue viscosity, and initial radius of each fusing bioink, respectively [22–24, 27]. Fig. 1 depicts the geometrical parameters that identify the characteristic fusion time. In experimental investigations, two bioinks (either spherical or cylindrical) can be placed close to each other, and the gradual fusion process can be recorded by acquiring images at different time points. Using digital image processing, the geometrical parameters described in Fig. 1 can be extracted, and τ can be found by using $(r/R)^2 = \sin^2\theta \approx 1 - \exp(-t/\tau)$. By plotting the $\sin^2\theta$ versus $(t - t_0/\tau)$ the characteristic fusion time can be obtained [23,24]. This quantitative evaluation can determine how fast or slow two bioinks fuse.

In an original revolutionary work, the characteristic fusion time was predicted using a comprehensive (theoretical, computational, and experimental) framework called cellular particle dynamics or CPD [23, 24]. Moreover, experimental results showed a faster fusion of bioink particles with cylindrical geometry compared to those with spherical shape. In this case, the effective characteristic fusion time for spherical bioinks was found 22 h whereas 10 h for cylindrical bioinks. However, the reason for this discrepancy was not clear. In other words, the lack of a microscopic model of fusion based on associated biological phenomena and the consequent lack of a mathematical framework prevented the tissue engineering community in general and bioprinting scientists in particular from calculating essential parameters such as energy and force of self-assembly in tissue maturation. To expedite the maturation procedure through bioinks fusion after bioprinting, first, we need to comprehend the fusion and establish mathematical relationships among involved parameters during this self-assembly phenomenon. We recently commenced close examination of the physics of self-assembly and developed a microscopic model of tissue fusion. We previously described the physics of fusion of spherical cellular bioinks and defined a tunable biophysical parameter in cellular bioinks for faster maturation of bioprinted tissues [27]. This model is based on the dynamics of cell adhesion molecules. Here, we generalize the microscopic model and physics of fusion for cylindrical bioinks. Using this generalized microscopic model, we provide a mathematical approach to comprehend the tissue fusion that can be used for faster maturation of bioprinted tissues. We employ statistical mechanics to establish the mathematical relation among associated parameters and determine the energy, force, and work in cell migration and cellular self-assembly during fusion. To that end, several canonical ensembles in terms of zipper models with ground- and excited-states are considered as open-link and closed-link cells, respectively. The model uses the chemistry of cell adhesion molecules and statistical mechanics for optimizing the bioink geometry to accelerate tissue maturation of bioprinted cellular constructs. These links are among adhesive molecules described in our microscopic model. Consequently, the partition function is determined and cellular self-assembly energies and forces are calculated and compared for different geometries of bioinks, and essential involved geometrical parameters are obtained to accelerate tissue maturation. This original microscopic model and series of zippers allow us to investigate the tissue fusion mathematically for the first time; this can be beneficial for controlling the tissue self-assembly and post bioprinting maturation.

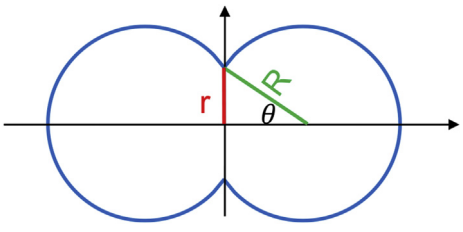

Fig. 1. Geometrical parameters necessary to study fusion of tissues quantitatively are r, R, and θ. Snapshot images from spherical and cylindrical bioinks are taken and analyzed using digital image processing to define r, R, and θ. Ultimately, characteristic fusion time can be determined from the graph $\sin^{(2)}\theta$ vs. time.

2. Materials and methods

2.1. Generalizing the microscopic model for fusion of bioinks with different geometries

In order to establish a mathematical formulation and better understanding of the fusion procedure, we developed a microscopic model based on the cell adhesion molecules. In previous work, we introduced the microscopic model and extrapolated a series of events at the cellular level during the fusion of two spherical bioinks [27]. Here, we generalize the microscopic model for the fusion of cylindrical bioinks and discuss the series of events occurring during their fusion. This generalization will help to understand the fusion of any bioink geometry and can be used to optimize the fusion procedure. In this case, we consider imaginary ribbons (and strips) of cells around the contact point (line) of two bioinks for spherical (and cylindrical) fusion. The fusion involves a cascade of cell attachments located on those imaginary ribbons (strips) around the contact point (line).

2.2. Mathematical formulation for cellular self-assembly

We employed different coordinate systems to investigate various geometries of bioinks. To establish a mathematical framework and formulation for the fusion procedure using the developed microscopic model, a canonical ensemble comprised of closed and open links between cell adhesion molecules was considered for cell-attachment of two-dimensional fusion. The partition function and energy were calculated. By integration over a line and around a disk for cylindrical and spherical bioinks, three-dimensional fusion was mathematically investigated. Ultimately, the cell density was examined and compared for different geometries. The results were able to explain the discrepancy in different fusion times for different bioink geometries observed in an experimental report [24].

2.3. Fusion of two spherical tissue-like cell aggregates (bioinks)

In previous work, we provided a model based on imaginary ribbons of cells for tissue fusion [27]. In brief, the model assumed that during the fusion of two spherical bioinks, cells from each bioink start to attach to the cells on the opposite aggregate. This procedure starts when the first pair of cells at the contact point of two bioinks break a proportion of bonds (up to 60% [19]) with adjacent cells on the same bioink and develop new bonds with cells in the opposite aggregate. Attachment of the first pair of cells bring a few cells located on an imaginary ribbon around them that in turn break bonds with cells on the same bioink and

develop new bonds with cells on the other bioink. The fusion process continues by a cascade of these cell-attachments while the radius of imaginary ribbons and the number of involved cells increases. Fig. 2 shows the fusion of two spherical bioinks and the imaginary ribbons of cells.

2.4. Fusion of two cylindrical tissue-like cell aggregates (bioinks)

To understand the self-assembly of cylindrical bioink, here we generalize the model of fusion for spherical bioinks. In this case, instead of a contact point, two bioinks have a contact line as long as ℓ which is the length of each bioink. Cells located on the contact line from each bioink start to break bonds from the cells on the same bioink and develop new bonds with adjacent cells on the contact line from the opposite bioink. After the completion of cell attachment in the initial contact line, cells from two imaginary strips (one above and one below the initial contact line) from each bioink will be located in the proximity of the counterpart cells on the other bioink. This cell-attachment continues until the fusion process is complete. Fig. 2 indicates the fusion of two cylindrical bioinks with imaginary strips.

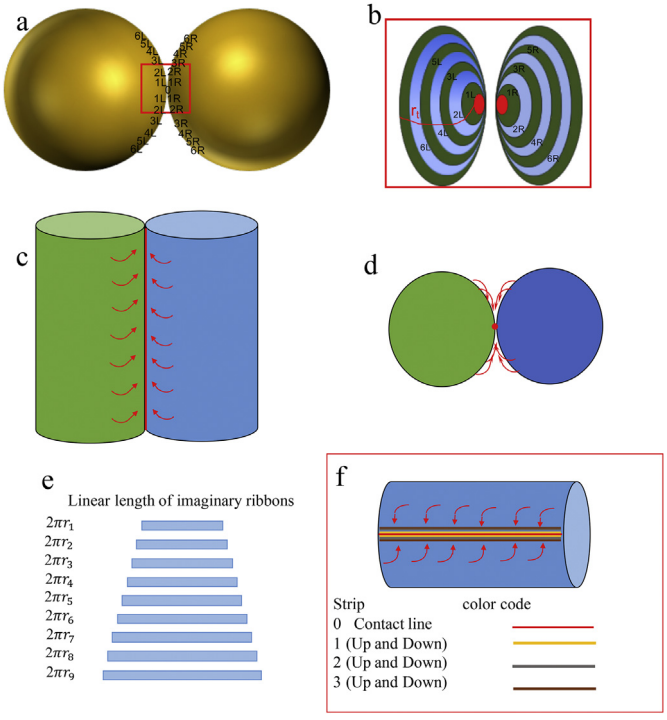

Fig. 2. Microscopic view of fusion procedure for two spherical and cylindrical bioinks. a) Spheroids start to fuse by a cascade of attachments of cells located on imaginary ribbons around the contact point of two bioinks. b) A closer look at the red square in part a. Cells on each ribbon on each bioink start developing bonds with cells on the opposite bioink, and after completion of cell-attachment in one ribbon, cells on the next ribbon approach the vicinity of the cells in the counterpart ribbon on the other bioink, and start attach. The radii of ribbons gradually enlarge until the fusion is complete. Adapted from Reference 27. c) Top-view of fusing cylindrical bioinks. Bioinks start to fuse by attachment of cells located on the contact line. d) Cross-sectional view of the cylindrical fusion. The red dot represents the cross-section of the contact line and the red arrows represent the cell movement throughout the fusion process. By the completion of attachment of the cells located on the contact line, cells on one imaginary strip above and one imaginary strip below the contact line from each bioink start to attach. e) The linear length of each ribbon is the circumference of the circle with radius r_i. In each step fusion, cells located on a pair of ribbons from both bioinks are involved in the attachment procedure. f) By the completion of attachment of cells in each strip, the next pair of strips will be closer to their counterparts on the other bioink and cells start to attach. The contact line is shown by red and each next pair of strips are displayed in different colors. (For interpretation of the references to color in this figure legend, the reader is referred to the Web version of this article.)

The fusion of bioinks is one critical step in a long series of sequences in the maturation of a bioprinted tissue; faster fusion can shorten the time needed for tissue/organ fabrication. Based on the experimental data for fusion of spherical and cylindrical bioinks [24], we compared the different geometries of bioinks and their impact on fusion. Considering the microscopic model of fusion described in Fig. 2, we define the forces that are applied to each cell during fusion in spherical and cylindrical coordinates for spherical and cylindrical bioinks respectively. It is worth noting that, based on our microscopic model, these forces exerted on cells originate in cell adhesion molecules and the extracellular matrix and correlate with the apparent tissue surface tension [27]. In a former work, we showed how higher surface tension could cause faster fusion resulting from more numerous and stronger bonds [27]. Here, the bioink geometry is examined mathematically, and we undertake constant surface tension for all bioinks. We consider the cellular motion powered by metabolic energy identical for different geometries of bioinks (as long as they are made from same cell type(s)) and associate the observed fusion time discrepancy in spheres and cylinders to the bioink geometries and consequent cellular attachments.

2.5. Cell adhesion molecules - building blocks of fusion

Usually, two cells cannot adhere per se because the surfaces of most cells are negatively charged, which would lead to repulsion, although the electrostatic repulsion is effective for no more than around 1 nm from the cell surface [28]. However, cell adhesion molecules are also presented and produce more long-lived bonds that, from the point of view of energy, are more favorable over nonspecific bonds. Specific bonds form only when the two cells are close enough (r_b). Just in this situation, highly cooperative multimolecular binding would happen that are caused by diffusion-dependent clustering of cell adhesion molecules [19]. Therefore, cells can adhere to each other.

Adhesive bond formation is associated with a reduction in the energy of the system. Therefore, one can determine the minimum energy of the system for the completion of the fusion procedure. Three different states can be considered for a cell adhesion molecule from one bioink called A and cell adhesion molecule from the opposite bioink called B [28]. In this case, A and B can be 1- free (ground state), 2- in an encounter complex of AB (transition state), or 3- bonded together and become C (excited state). This can be shown as:

$$A + B \leftrightarrows AB \leftrightarrows C.$$

When a chemical bond forms, the energy is released. In our microscopic model, the produced energy is consumed to bring subsequent cell adhesion molecules to transition and excited states in a cascade of reactions during cell-attachments. As such, once cells are in close vicinity to each other, as described in Fig. 2, their adhesion molecules are in a transition state, and consequently an excited state and develop new bonds. These reactions provide enough energy for the movement of cells located on upcoming imaginary ribbons or strips (for spheres and cylinders, respectively). To mathematically investigate these chemical reactions of cell adhesion molecules and their different states, we use the zipper model and statistical mechanics.

2.6. Zipper model to establish a mathematical formulation of fusion

To investigate bioink fusion, we consider the cascade of cell-attachments as a closing zipper model. The zipper model was first solved by Charles Kittel [29] and is now well established among physicists. Here, we use the zipper model to find energy and force involved in self-assembly of multicellular systems. Using the zipper model helps to simplify the complex procedure of multicellular self-assembly in the maturation procedure and helps to examine the self-assembly process

mathematically. Therefore, we can determine the partition function describing the statistical properties of the system by considering the ensemble of closing links between cells from each bioink. In this case, each link can be either open with energy zero (ground state) or closed with energy ε (excited state). The transition state is considered as zero energy. This closing should be in one direction only, that is the fusing direction– the N^{th} link can be closed only when the $(N\text{-}1)^{th}$ is closed. To that end, we can write the partition function as:

$$Z = \sum_{i=0}^{n} e^{-E_i/k_B T} = \sum_{i=0}^{n} e^{-\beta E_i}.$$

where i is the index for the microstate of the system which is the attachment of each pair of cells, k_B is the Boltzmann constant, T is the temperature in Kelvin, β is the thermodynamic beta, and E_i is the total energy of the system in the respective microsystem (that is ε for all closed links) [29]. Therefore:

$$Z = e^{-\beta.0} + e^{-\beta.1\varepsilon} + e^{-\beta.2\varepsilon} + \ldots + e^{-(N-1)\beta\varepsilon} + e^{-N\beta\varepsilon}.$$

One can use the relation $1 + r + r^2 + \ldots + r^{N-1} + r^N = \frac{1-r^{N+1}}{1-r^N}$; by considering $r = e^{-\beta\varepsilon}$ we can represent the partition function as:

$$Z = \frac{1 - e^{-\beta(N+1)\varepsilon}}{1 - e^{-\beta\varepsilon}}$$

By finding the partition function of our ensemble, we are now able to determine many macroscopic thermodynamic variables. Here we identify the average energy for a complete zipping process through the partial derivative of the partition function with respect to the thermodynamic beta.

$$\langle E\rangle = -\frac{\partial \log Z}{\partial\beta} = -\frac{1}{Z}\frac{\partial Z}{\partial\beta} = -\frac{1}{Z}\frac{\partial}{\partial\beta}\frac{1 - e^{-\beta(N+1)\varepsilon}}{1 - e^{-\beta\varepsilon}}$$
$$= -\frac{\varepsilon(N+1)e^{-(N+1)\beta\varepsilon}}{1 - e^{-(N+1)\beta\varepsilon}} + \frac{\varepsilon e^{-\beta\varepsilon}}{1 - e^{-\beta\varepsilon}} \quad (1)$$

As depicted in Fig. 3, the fusion of cylinders and spheres can be shown as a set of zippers.

The total energy of the self-assembly, $\langle E\rangle_{total}$, is determined by the summation of $\langle E\rangle$ from 0 to 2π for spherical aggregates, and from $-\ell/2$ to $\ell/2$ for cylindrical bioinks (Fig. 3). Therefore, $\langle E\rangle_{total}$ will be equal to $\langle E\rangle$ multiplied by the number of zippers present in cylinders or spheres. The number of zippers is defined as the length divided by the distance between subsequent adhesive molecules (κ). Thus, the κ depends on the tissue as well as the size of cells on the surface of the bioink. The total energy produced by adhesive bonds and consumed by cell migration (self-assembly) will be determined as:

$$\langle E\rangle_{total} = number\ of\ zippers\ \times \langle E\rangle \quad (2)$$

By substituting $\langle E\rangle$ from Eq. [1] in Eq. [2] for both spheres and cylinders we can determine the total energy for self-assembly.

The fusion of spheroids encompasses numerous zippers, all with the starting point at the center of the fusion cross-section disk, the contact point. Therefore, the number of zippers is determined by the circumference of the disk divided by the κ. Therefore,

$$\langle E\rangle_{total\ for\ sph} = \frac{2\pi r}{\kappa}\langle E\rangle = \frac{-2\pi r}{\kappa}\left(\frac{\varepsilon(N+1)e^{-(N+1)\beta\varepsilon}}{1 - e^{-(N+1)\beta\varepsilon}} + \frac{\varepsilon e^{-\beta\varepsilon}}{1 - e^{-\beta\varepsilon}}\right) \quad (3)$$

Nevertheless, it is worth noting that for cylindrical $\langle E\rangle_{total}$ determined from the summation is just for fusing parts above the contact line and a multiplication factor of two can give the final average energy for cylinders. Therefore,

$$\langle E\rangle_{total\ for\ cyl} = \frac{2\ell}{\kappa}\langle E\rangle = \frac{-2\ell}{\kappa}\left(\frac{\varepsilon(N'+1)e^{-(N'+1)\beta\varepsilon}}{1 - e^{-(N'+1)\beta\varepsilon}} + \frac{\varepsilon e^{-\beta\varepsilon}}{1 - e^{-\beta\varepsilon}}\right) \quad (4)$$

3. Results and discussions

Previous experimental results showed different characteristic fusion time for two different bioink geometries (spherical and cylindrical bioinks) [24]. In this paper, we have developed a microscopic model based on cell adhesion molecules to describe the fusion procedure. Using statistical mechanics, we have considered a series of zippers to determine the energy of cellular self-assembly. The first law of thermodynamics states that the change in internal energy of a system is equal to the difference in the heat added to that system and the work done by the system (W). In the case of fusing bioinks, the internal energy of the system is zero due to the constant temperature (37 $^{\circ}C$ in tissue culture incubators). Therefore, the energy produced in chemical reactions ($\langle E\rangle_{total}$) is consumed for the work of moving cells to the vicinity of counterpart cells in the opposite bioink

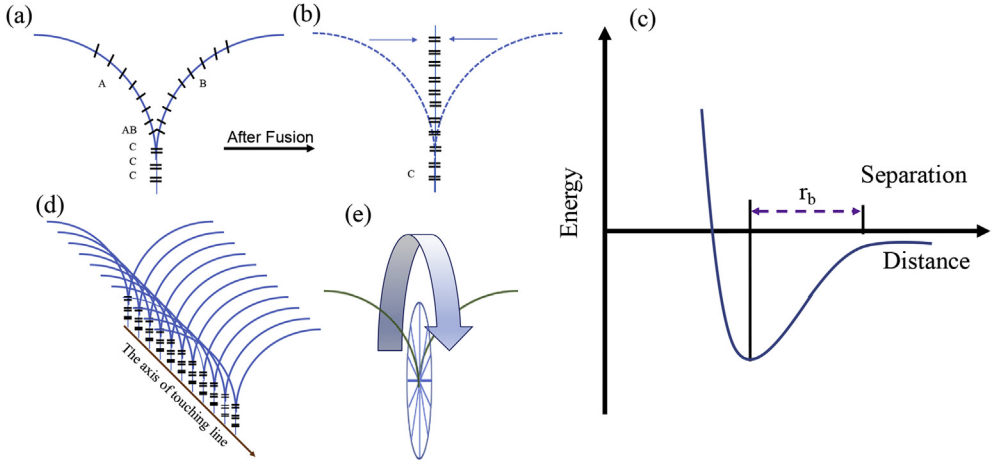

Fig. 3. Zipper model for fusion of tissue like cell aggregates (bioinks). a) A zipper model consists of two sequences of adhesion molecules from two bioinks. Each adhesion molecule can develop a bond with its counterpart on the other bioink and release energy. In this case, if adhesion molecule A is far from adhesion molecule B they are open (ground state energy is zero). If they become closer, they make an intermediate state called AB (still the energy is zero). If A and B become close enough (around r_b) they can become a closed link and make a bond, C (excited state and the energy is ε). b) As the fusion continues, more A and B molecules develop bonds and release energy. The dashed lines depict the initial location of adhesion molecules and cells. The solid vertical line demonstrates the final closed zipper when the bioinks complete the fusion process. c) Shows the energy versus distance. d) A series of zippers on a line (contact line) for two cylindrical bioinks. The same configuration can be considered for below the line. e) A series of zippers around the contact point for fusion of spherical bioinks.

$$W = Fd = \langle E \rangle_{total} \tag{5}$$

where F represents the force and d is the displacement done by the work (W). The time for rupturing/developing a bond can be determined using the Bell equation [19,28]:

$$\tau = \tau_0 \exp(-\alpha f / K_B T) \tag{6}$$

On the other hand, this time would be taken by two sequential cells from different bioinks to migrate to the proximity of each other for new cell attachment. Here we assume the distance that each cell should be relocated to get to the vicinity of counterpart cell is $d = \frac{D-r_b}{2}$, where D is the initial distance between two cells on different bioinks, then we will have $t = d/v$ and by substituting $t = \tau$ in Eq. [6], we would have:

$$Ln\, d/v\tau_0 = -\alpha f / K_B T \rightarrow f = \frac{K_B T}{\alpha} Ln\, v\tau_0/d$$

where τ_0 is the average lifetime of the adhesion bond and α is a parameter with units of length, and its value must be obtained empirically.

Therefore, the Bell equation gives this comparison:

$$f = \frac{K_B T}{\alpha} Ln\, v\tau_0/d \rightarrow \frac{f_{cyl}}{f_{sph}} = \frac{\alpha_{sph}}{\alpha_{cyl}} \frac{Ln\, v_{cyl}\tau_0/d}{Ln\, v_{sph}\tau_0/d}.$$

One can argue that τ_0 and d can be considered equal in both cases for simplification and the ratio of both α s can be considered as a constant B. Therefore,

$$\frac{f_{cyl}}{f_{sph}} \approx \frac{Ln\, v_{cyl}}{Ln\, v_{sph}} \tag{7}$$

This shows that the greater magnitude of force will provide faster fusion. To compare the force, based on Eq. [5], we can compare the $\langle E \rangle_{total}$ for both spherical and cylindrical fusions in Eq. [3] and [4]. It is evident that the N, which is the number of closed links, would determine the higher energy and force.

There are two ways to compare the N (number of closed links) for fusion of spherical and cylindrical bioinks: 1) comparing the microscopic models and 2) comparing surface cell density in different coordinates.

3.1. Comparing microscopic models

By comparing the microscopic model in spherical and cylindrical cases (Fig. 2), it is notable that the numbers of engaged cells are different in different geometries in each time-point. Except for the beginning of fusion that occurs by the attachment of cells in a line, the rest of the procedure includes two lines of cells from each bioink in the cylindrical case. In the spherical case, however, the circumference of each ribbon increases throughout the fusion and the number of engaged cells in each time-point is higher than the previous time-point (Table 1).

Based on the zipper model and the calculated energy (Eq. [3] and [4]) in addition to data in Fig. 2e and Table 1, which show that the number of links are initially much less in spherical models and gradually increases the force for spherical fusion is much less than that of cylindrical fusion specifically during early hours. Consequently, fusion of spherical bioinks is slower than that in cylindrical bioinks; confirming the experimental data [24] in first 10 h the fusion of cylindrical bioinks reach ~70% of its maximum whereas spherical bioinks reach 20% of complete fusion.

3.2. Comparing surface cell density

The fusion process encompasses the attachment of cells; therefore, the number of cells (in fact the consequent number of adhesion molecules) is an essential factor in its completion. Each cell has adhesive molecules that are the building units of cell bonding and attachment during fusion. Therefore, surface cell density should be investigated and compared for different geometries. Considering the cell density "C" as the integration of several infinitesimal units of cell density represented by dc, the surface cell density becomes $\sigma = dc/da$, where σ is the surface cell distribution and da is the area element.

Table 1
The contact area for two cylindrical bioinks, while fusing, is a line with length ℓ at the beginning and two lines with length ℓ in following time-points. However, for spherical bioinks the contact area is a point at the beginning, and in following time points, it is a ribbon with a linear length of $2\pi r_t$ where r_t increases over time. Therefore, the contact area for cells involved in the process of cell-attachment is much more significant for cylindrical bioinks. This is specifically notable for the beginning of the fusion process when the number of involved cells in spherical bioinks are much less.

Time	Spherical	Cylindrical
0	2cells	Cells on a strip with length ℓ
1	Cells on ribbon with length $2\pi r_1$	Cells on 2 strips with length ℓ
2	Cells on ribbon with length $2\pi r_2$	Cells on 2 strips with length ℓ
3	Cells on ribbon with length $2\pi r_3$	Cells on 2 strips with length ℓ
4	Cells on ribbon with length $2\pi r_4$	Cells on 2 strips with length ℓ
5	Cells on ribbon with length $2\pi r_5$	Cells on 2 strips with length ℓ
6	Cells on ribbon with length $2\pi r_6$	Cells on 2 strips with length ℓ
7	Cells on ribbon with length $2\pi r_7$	Cells on 2 strips with length ℓ
8	Cells on ribbon with length $2\pi r_8$	Cells on 2 strips with length ℓ

In the spherical coordinate, (ρ, θ, φ) are radial distance, polar angle, and azimuthal angle, respectively where $0 < \theta < \pi$, and $0 < \varphi < 2\pi$. In the cylindrical coordinate system, we can show each point with (ρ, ψ, z) that represent radial distance, azimuthal angle, and vertical distance where $0 < \psi < 2\pi$. Consequently, in the spherical coordinate system, the surface element can be written as

$$da_{sph} = \rho^2 \sin\theta d\theta d\varphi \hat{\rho} + \rho \sin\theta d\varphi d\rho \hat{\theta} + \rho d\theta d\rho \hat{\varphi}$$

This long expression of area element in the spherical coordinate can be simplified by considering the fact that the radius of the sphere is constant ($d\rho = 0$); therefore, in the directions of $\hat{\theta}$ and $\hat{\varphi}$ the magnitude would become zero. Consequently, cell density can be written as:

$dc_{sph} = \sigma\rho^2 \sin\theta d\theta d\varphi$ in $\hat{\rho}$ direction.

The cell density can be obtained by integration of all dc. Therefore:

$$C_{sph} = \int dc_{sph} = \iint \sigma\rho^2 \sin\theta d\theta d\varphi = \sigma\rho^2 \iint \sin\theta d\theta d\varphi = 2\sigma\rho^2 \int_0^{2\pi} d\varphi = 4\sigma\pi\rho^2$$

It is clear that we considered the cell density as a vector instead of a scalar. This cell density vector with the direction of $\hat{\rho}$ is based on the adhesion molecules of the cells described in the microscopic model in Fig. 2 that confirms the connection of the one-to-one pair of cell adhesion molecules from both bioinks. This means each molecule would develop only one bond with only one other molecule from the other bioink only when they are in the vicinity of each other (both in $\hat{\rho}$ direction). In other words, cells located on each imaginary ribbon or strip (in case of a sphere or cylinder) can start developing bonds with their counterpart on the opposite bioink using their adhesion molecules in the direction of $\hat{\rho}$ which is a particular point to fulfill the condition for both molecules.

The area element for the Cylindrical coordinate is:

$$da_{cyl} = \rho d\psi dz \hat{\rho} + d\rho dz \hat{\psi} + \rho d\rho d\psi \hat{z}$$

Using the same assumption of the constant radius will change it to:

$da_{cyl} = \rho d\psi dz$ only in $\hat{\rho}$ direction.

Hence, the cell density for the cylindrical coordinate system becomes:

$$C_{cyl} = \int dc = \int \sigma' \rho d\psi dz = \sigma' \rho \iint d\psi dz = \sigma' \rho \int \int_0^{2\pi} dz d\psi = \sigma' \rho 2\pi \int_{-\ell/2}^{\ell/2} dz = \sigma' \rho 2\pi \ell$$

where σ', ρ, ℓ are the surface cell distribution, radius, and length of cylinders, respectively. By comparing the surface cell density in the spherical and cylindrical coordinate systems, we can determine $2\sigma\rho_{sph}^2 = \sigma'\rho_{cyl}\ell$ and considering the identical radii for cylinders and spheroids ($\rho_{Sph} = \rho_{cyl}$) we arrive at $\rho = \ell\sigma'/2\sigma$. This equation can be further simplified by considering the surface tensions to be identical for both bioinks, which means they are prepared using the same method. We previously showed, experimentally, that it is the preparation method that controls the surface tension [27]. In addition, it has been shown that the $\gamma \approx aJn$ where a is a dimensionless constant, J is the effective binding energy among cell adhesion molecules, and n is the number of these contacts per unit area [21]. Assuming equal n for the same type of cells, we can conclude that surface tension is related to the surface cell density $\gamma \approx b\sigma$, where b is a constant. Therefore, by considering the same surface tension for both geometries of bioinks ($\gamma = \gamma' \rightarrow \sigma = \sigma'$), we can simplify the surface cell density equations to

$$C_{sph} = C_{cyl} \rightarrow \rho = \ell/2$$

This calculation provides very useful information regarding the size of the bioink with different geometries. In order to get the same surface cell density for spherical and cylindrical bioinks, the radius of the cylinder should be as long as half of the length of the cylinder. However, in reality, the length of a cylinder is always much larger than its radius. Therefore, the C_{cyl} is always much more significant than C_{sph}. This indicates that the fusion of cylinders is more favorable as far as cell density is concerned, which in turn relates to the number of cell adhesive molecules, energy, and force involved in self-assembly. In this calculation, we considered the same surface tension (and consequently $\sigma = \sigma'$). However, this mathematical framework can be used to compare bioinks with different surface tensions as well, provided that the surface tension of the bioinks are known. The experimental evaluation of tissue tensiometry is described in Ref. 27.

4. Conclusion

Understanding the principles of self-assembly and dynamics of multicellular systems based on the biological physics of embryonic development is key to the accelerated maturation of bioprinted biological constructs. We previously introduced a tunable physical parameter called the apparent tissue surface tension for faster maturation and elaborated on the fusion of spherical bioinks. Here, we generalized the microscopic model for fusion of cylindrical bioinks. Furthermore, a mathematical framework was developed to investigate tissue fusion and cellular self-assembly that helps to evaluate the effect of bioink geometry on maturation time in the post-bioprinting procedure. By comparing exerted forces on cells as well as surface cell density in spherical and cylindrical coordinate systems, we showed the reasons for discrepancies in the maturation procedure. These microscopic models of fusion (both cylindrical and spherical bioinks) in addition to mathematical investigations of fusion can assist in designing different bioink novel geometries to optimize tissue biofabrication using bioprinters.

Acknowledgment

Authors would like to thank Drs. Jareer Kassis, Mohammad Sherafati, Mohammad Valizadeh, and Carlos Kengla.

Declaration of conflicting interests

The authors declared that they had no conflicts of interest with respect to their authorship or the publication of this article.

References

[1] A. Shafiee, M.M. Salleh, M. Yahaya, Fabrication of organic solar cells based on a blend of donor-acceptor molecules by inkjet printing technique, in: IEEE International Conference on Semiconductor Electronics, ICSE, 2008, pp. 319–322, https://doi.org/10.1109/SMELEC.2008.4770332.
[2] P. Calvert, Inkjet printing for materials and devices, Chem. Mater. 13 (10) (2001) 3299–3305, https://doi.org/10.1021/cm0101632.
[3] A. Shafiee, M. Mat Salleh, M. Yahaya, Fabrication of organic solar cells based on a blend of poly (3-octylthiophene-2, 5-diyl) and fullerene derivative using inkjet printing technique, in: SPIE Proceedings, 7493, 2009, p. 74932D, https://doi.org/10.1117/12.843467.
[4] S. Khan, L. Lorenzelli, R.S. Dahiya, Technologies for printing sensors and electronics over large flexible substrates: a review, IEEE Sens. J. 15 (2015) 3164–3185, https://doi.org/10.1109/JSEN.2014.2375203.
[5] W.Z. Samad, M.M. Salleh, A. Shafiee, M.A. Yarmo, Preparation nanostructure thin films of fluorine doped tin oxide by inkjet printing technique, in: AIP Conference Proceedings, vol. 1284, 2010, pp. 83–86, https://doi.org/10.1063/1.3515569.
[6] W.Z. Samad, M.M. Salleh, A. Shafiee, M.A. Yarmo, Transparent conducting thin films of fluoro doped tin oxide (FTO) deposited using inkjet printing technique, in: IEEE International Conference on Semiconductor Electronics, ICSE 2010, 2010.
[7] W.Z. Samad, M.M. Salleh, A. Shafiee, M.A. Yarmo, Transparent conductive electrode of fluorine doped tin oxide prepared by inkjet printing technique, Mater. Sci. Forum 663–665 (2010) 694–697, https://doi.org/10.4028/www.scientific.net/MSF.663-665.694.
[8] N.I. Moldovan, N. Hibino, K. Nakayama, Principles of the KenzanMethod for robotic cell spheroid-based three-dimensional bioprinting, Tissue Eng. B Rev. 23 (3) (2017) 237–244, https://doi.org/10.1089/ten.teb.2016.0322.
[9] H.-W. Kang, S.J. Lee, I.K. Ko, C. Kengla, J.J. Yoo, A. Atala, A 3D bioprinting system to produce human-scale tissue constructs with structural integrity, Nat. Biotechnol. 34 (3) (2016) 312–319, https://doi.org/10.1038/nbt.3413.
[10] F.T.C. Moreira, R.A.F. Dutra, J.P. Noronha, M.G.F. Sales, Novel sensory surface for creatine kinase electrochemical detection, Biosens. Bioelectron. 56 (c) (2014) 217–222, https://doi.org/10.1016/j.bios.2013.12.052.
[11] P. Mostafalu, W. Lenk, M.R. Dokmeci, B. Ziaie, A. Khademhosseini, S.R. Sonkusale, Wireless flexible smart bandage for continuous monitoring of wound oxygenation, IEEE Trans Biomed Circuits Syst 9 (5) (2015) 670–677, https://doi.org/10.1109/TBCAS.2015.2488582.
[12] A. Shafiee, E. Ghadiri, J. Kassis, N. Pourhabibi Zarandi, A. Atala, Biosensing technologies for medical applications, manufacturing, and regenerative medicine, Curr Stem Cell Rep 4 (2) (2018) 105–115, https://doi.org/10.1016/j.molmed.2016.01.003.
[13] C.J. Ferris, K.G. Gilmore, G.G. Wallace, Het Panhuis M. Biofabrication: an overview of the approaches used for printing of living cells, Appl. Microbiol. Biotechnol. 97 (10) (2013) 4243–4258, https://doi.org/10.1007/s00253-013-4853-6.
[14] S.V. Murphy, A. Atala, 3D bioprinting of tissues and organs, Nature Publishing Group 32 (8) (2014) 773–785, https://doi.org/10.1038/nbt.2958.
[15] A. Shafiee, A. Atala, Printing technologies for medical applications, Trends Mol. Med. 22 (3) (2016) 254–265, https://doi.org/10.1016/j.molmed.2016.01.003.
[16] A. Shafiee, A. Atala, Tissue engineering: toward a new era of medicine, Annu. Rev. Med. 68 (2017) 29–40, https://doi.org/10.1146/annurev-med-102715-092331.
[17] C. Norotte, F.S. Marga, L.E. Niklason, G. Forgacs, Scaffold-free vascular tissue engineering using bioprinting, Biomaterials 30 (30) (2009) 5910–5917, https://doi.org/10.1016/j.biomaterials.2009.06.034.
[18] L. Moldovan, C.M. Babbey, M.P. Murphy, N.I. Moldovan, Comparison of biomaterial-dependent and -independent bioprinting methods for cardiovascular medicine, Current Opinion in Biomedical Engineering 2 (2017) 124–131, https://doi.org/10.1016/j.cobme.2017.05.009.
[19] G. Forgacs, S.A. Newman, Biological Physics of the Developing Embryo, 2005.
[20] M.S. Steinberg, Reconstruction of tissues by dissociated cells, Science 141 (3579) (1963) 401–408.
[21] G. Forgacs, R.A. Foty, Y. Shafrir, M.S. Steinberg, Viscoelastic properties of living embryonic tissues: a quantitative study, Biophys. J. 74 (5) (1998) 2227–2234.
[22] I. Kosztin, G. Vunjak-Novakovic, G. Forgacs, Colloquium: modeling the dynamics of multicellular systems: application to tissue engineering, Rev. Mod. Phys. 84 (4) (2012) 1791–1805, https://doi.org/10.1103/RevModPhys.84.1791.
[23] M. McCune, A. Shafiee, G. Forgacs, I. Kosztin, Predictive modeling of post bioprinting structure formation, Soft Matter 10 (11) (2014) 1790–1800, https://doi.org/10.1039/c3sm52806e.
[24] A. Shafiee, M. McCune, G. Forgacs, I. Kosztin, Post-deposition bioink self-assembly: a quantitative study, Biofabrication 7 (4) (2015), 045005, https://doi.org/10.1088/1758-5090/7/4/045005.
[25] R.A. Foty, M.S. Steinberg, Differential adhesion in model systems, WIREs Dev Biol 2 (5) (2013) 631–645, https://doi.org/10.1002/wdev.104.
[26] R.A. Foty, M.S. Steinberg, The differential adhesion hypothesis: a direct evaluation, Dev. Biol. 278 (1) (2005) 255–263, https://doi.org/10.1016/j.ydbio.2004.11.012.
[27] A. Shafiee, C. Norotte, E. Ghadiri, Cellular bioink surface tension: a tunable biophysical parameter for faster maturation of bioprinted tissue, Bioprinting 8 (2017) 13–21, https://doi.org/10.1016/j.bprint.2017.10.001.
[28] G. Bell, Models for the specific adhesion of cells to cells, Science 200 (4342) (1978) 618–627, https://doi.org/10.1126/science.347575.
[29] C. Kittel, Phase transition of a molecular zipper, Am. J. Phys. 37 (9) (1969) 917–920, https://doi.org/10.1119/1.1975930.